Fate mapping reveals origin and dynamics of lymph node follicular dendritic cells

Meryem Jarjour,[1,2,3,4] Audrey Jorquera,[1,2,3,4] Isabelle Mondor,[1,2,3,4] Stephan Wienert,[5] Priyanka Narang,[6] Mark C. Coles,[6] Frederick Klauschen,[5] and Marc Bajénoff[1,2,3,4]

[1]Centre d'Immunologie de Marseille-Luminy (CIML), Aix-Marseille Université, UM2 Marseille, France
[2]Institut National de la Santé et de la Recherche Médicale (INSERM), UMR_S 1104 Marseille, France
[3]Centre National de la Recherche Scientifique (CNRS), UMR7280 Marseille, France
[4]Aix-Marseille Univ (AMU), F-13284 Marseille, France
[5]Institute of Pathology, Charité Universitätsmedizin Berlin, 10117 Berlin, Germany
[6]Center for Immunology and Infection, Department of Biology and Hull York Medical School, University of York, YO10 5DD York, England, UK

Follicular dendritic cells (FDCs) regulate B cell function and development of high affinity antibody responses but little is known about their biology. FDCs associate in intricate cellular networks within secondary lymphoid organs. In vitro and ex vivo methods, therefore, allow only limited understanding of the genuine immunobiology of FDCs in their native habitat. Herein, we used various multicolor fate mapping systems to investigate the ontogeny and dynamics of lymph node (LN) FDCs in situ. We show that LN FDC networks arise from the clonal expansion and differentiation of marginal reticular cells (MRCs), a population of lymphoid stromal cells lining the LN subcapsular sinus. We further demonstrate that during an immune response, FDCs accumulate in germinal centers and that neither the recruitment of circulating progenitors nor the division of local mature FDCs significantly contributes to this accumulation. Rather, we provide evidence that newly generated FDCs also arise from the proliferation and differentiation of MRCs, thus unraveling a critical function of this poorly defined stromal cell population.

CORRESPONDENCE
Marc Bajénoff:
bajenoff@ciml.univ-mrs.fr

Abbreviations used: EdU, 5-ethynyl-2′-deoxyuridine); FDC, follicular DC; FRC, fibroblastic reticular cell; GC, germinal center; LTi, lymphoid tissue inducer; MAdCAM-1, mucosal vascular addressin cell adhesion molecule 1; MRC, marginal reticular cell; RANK-L, receptor activator of NF-κB ligand; SCS, subcapsular sinus; SLO, secondary lymphoid organ; VSC, versatile stromal cell.

Follicular DCs (FDCs) represent the follicular stromal cell compartment in charge of organizing B cell homeostasis and immune responses in secondary lymphoid organs (SLOs), including the development and production of high affinity antibodies. In the absence of FDCs, B cells would not migrate, form follicles, or mount humoral immune responses (Cyster et al., 2000; Bajénoff et al., 2006; Allen and Cyster, 2008; Wang et al., 2011).

FDCs were characterized decades ago as large follicle-associated dendritic-like cells displaying multiple long centrifugal processes in constant interaction with B cells (Szakal and Hanna, 1968; Chen et al., 1978; Klaus et al., 1980; Mandel et al., 1981). They secrete the B cell follicle homing chemokine CXCL13 and constitute a cellular scaffold for B cell migration (Ansel et al., 2000; Bajénoff et al., 2006). During immune responses, FDCs act as antigen-presenting and -retaining cells that remodel the primary follicular network into germinal centers (GCs), a specialized structure in which B cells proliferate, undergo somatic hypermutation, and carry out class switching (Allen et al., 2007; Garin et al., 2010; Victora and Nussenzweig, 2012). Elucidating FDC biology is thus critical for a better understanding of humoral immunity.

Although several studies brought definitive evidence of the mesenchymal origin of FDCs (Endres et al., 1999; Muñoz-Fernández et al., 2006; Wilke et al., 2010; Krautler et al., 2012), the identity and localization of LN FDC progenitors remain unknown. Krautler et al. (2012) described a population of splenic perivascular mural cells that express Mfge8 (milk fat globule–EGF factor 8 protein) and NG2, respond to LTβR signals, depend on lymphoid tissue inducer (LTi) cells, and are capable of generating FDC networks. Importantly, the so-called mural pre-FDCs are absent from LN stroma based on

The Rockefeller University Press $30.00
J. Exp. Med. 2014 Vol. 211 No. 6 1109-1122
www.jem.org/cgi/doi/10.1084/jem.20132409

The Journal of Experimental Medicine

published markers (not depicted). Using lineage tracing and transplant experiments, Castagnaro et al. (2013) reported that the Nkx2-5$^+$ Islet-1$^+$ mesenchymal lineage gave rise to splenic fibroblastic reticular cells (FRCs), FDCs, marginal reticular cell (MRCs), and mural cells but was not involved in the generation of LN and Peyer's patch stroma. Although these studies identified the ontogenic precursors of splenic FDCs, they did not address the origin of LN FDCs. Therefore, LN and splenic FDCs appear to rely on different developmental mechanisms and caution should be paid when extrapolating conclusions obtained from one organ to the other.

Shortly after birth, the very first BM-derived B cells invade neonatal LNs, triggering the primary development of lymphoid follicles (van Rees et al., 1985; Bajénoff and Germain, 2009). A few weeks later, follicles mature and accumulate FDCs associated in intricate 3D meshworks. Once established, FDC networks are not rigid matrices but are still able to undergo tremendous remodeling. For instance, upon inflammation, adult FDC networks rapidly remodel to support GC development but the cellular mechanisms underlying this crucial phase of FDC biology remain elusive. In summary, we still don't know whether the initial establishment of the LN FDC network and its subsequent remodeling rely on the recruitment and/or the local proliferation of either mature FDCs or unknown precursors belonging to the FDC lineage.

Why do we know so little about LN FDC biology? FDCs are rare, stellate, and highly interconnected cells, meant to function as large 3D networks that are very difficult to isolate and culture from nonmanipulated LNs (Muñoz-Fernández et al., 2006; Wilke et al., 2010; Usui et al., 2012). Therefore, in vitro methods only offer a limited understanding of the genuine immunobiology of FDCs in their complex native environment.

The recent development of multicolor fate mapping systems based on Cre-lox technology has created new tools to study cell dynamics in situ (Livet et al., 2007; Snippert et al., 2010; Tabansky et al., 2013). Here, we used various multicolor fate-mapping systems to track LN FDCs in vivo and unravel key features of LN FDC ontogeny and remodeling during inflammation.

RESULTS

LN FDCs derive from the proliferation of tissue-resident progenitors of mesenchymal origin

To investigate the origin and dynamics of LN FDCs, we developed a series of multicolored fate mapping systems in which FDCs, or their progenitors, stochastically acquire fluorescent markers and transmit them to their progeny. To this aim, we developed the Ubow mouse in which the Brainbow 1.0L construct (Livet et al., 2007), which allows combinatorial expression of three fluorescent proteins (dTomato, CFP, and YFP), is under the control of the human Ubiquitin-C promoter (Ghigo et al., 2013). In Ubow mouse, all cells express dTomato in the absence of CFP or YFP expression. Any Ubow cell that coexpresses the Cre recombinase undergoes a single and definitive recombination event leading to the loss of dTomato expression and the stochastic acquisition of YFP or CFP expression. Importantly, this choice is definitive, even in constitutively Cre-expressing cells, hence allowing Ubow cells to stochastically acquire a certain color for their entire lifespan and transfer it to their progeny (fate mapping). If daughter cells settle nearby their colored progenitor, they generate foci of monocolored cells (Ghigo et al., 2013).

To investigate the ontogeny of LN FDC networks and unravel the nature of their progenitors, we crossed the Ubow mouse to the Wnt-1Cre transgenic mouse, widely used to map the fate of neural crest cells, a transient, multipotent, migratory cell population that gives rise to the head and neck mesenchymal structures (Jiang et al., 2000; Fig. 1 A). If FDCs arose from local mesenchymal progenitors, we expected the Wnt-1Cre Ubow$^{+/-}$ upper LN (auricular and cervical) FDC networks to express CFP and YFP while the lower LN (inguinal and popliteal) FDC networks should continue to express dTomato in absence of Cre expression. However, if neural crest–derived cells migrate after their mesenchymal differentiation beyond the head- and neck-related organs, CFP and YFP FDCs should also be observed in the lower LNs of these mice. Confocal analysis of Wnt-1Cre Ubow$^{+/-}$ mice upper LNs revealed that all mature CD21/35$^+$ FDCs expressed CFP (30%) or YFP (70%; Fig. 1, A and B, left).

We then analyzed the lower LNs of the same mice and observed that all their FDCs exclusively expressed dTomato (Fig. 1 B, left). Therefore, the primary development of LN FDC networks relies on local noncirculating precursors, just as in splenic white pulp development (Castagnaro et al., 2013).

Importantly, the CFP$^+$ and YFP$^+$ FDCs in the upper LNs of Wnt-1Cre Ubow$^{+/-}$ were not randomly distributed but rather aggregated into mutually exclusive monocolored foci (Fig. 1 B, left). Despite the fact that the recombination events leading to CFP and YFP expression from the Ubow construct are purely stochastic, we consistently observed a bias toward YFP expression in the Wnt-1Cre Ubow$^{+/-}$ stromal cells. This bias was also observed in B cells and myeloid cells of Ubow mice crossed to reporter mice in which those cell types specifically express Cre (not depicted; Ghigo et al., 2013), suggesting this is an intrinsic feature of the Ubow construct.

As CFP$^+$ FDCs represented only 30% of all FDCs in Wnt-1Cre Ubow$^{+/-}$ mice, we expected the frequency of CFP^{++} FDCs in Wnt-1Cre Ubow$^{+/+}$ mice to be ∼9% (i.e., 30% of 30%). In this case, the recombination bias observed in the Ubow mouse would represent a unique advantage to track the behavior of very few cells belonging to a much larger population. Analysis of the upper LNs from Wnt-1Cre Ubow$^{+/+}$ mice that express two copies of the Ubow transgene indicated that their FDCs segregated into YFP^{++} (58%), CFP$^+$YFP$^+$ (31%), and CFP^{++} (11%) populations (Fig. 1 A). As CFP^{++} FDCs were the rarest colored cells in those LNs, we aimed to determine if they were randomly distributed within follicles or associated in clusters. As depicted in the right panel of Fig. 1 B, CFP^{++} FDCs were also gathered in monocolored foci within follicles. Applying our software tool ClusterQuant to the raw confocal datasets, it clearly appeared that CFP^{++} clusters organized in a nonrandom fashion (Ghigo et al., 2013; Materials and methods; Fig. 1, C and D; and Fig. S1).

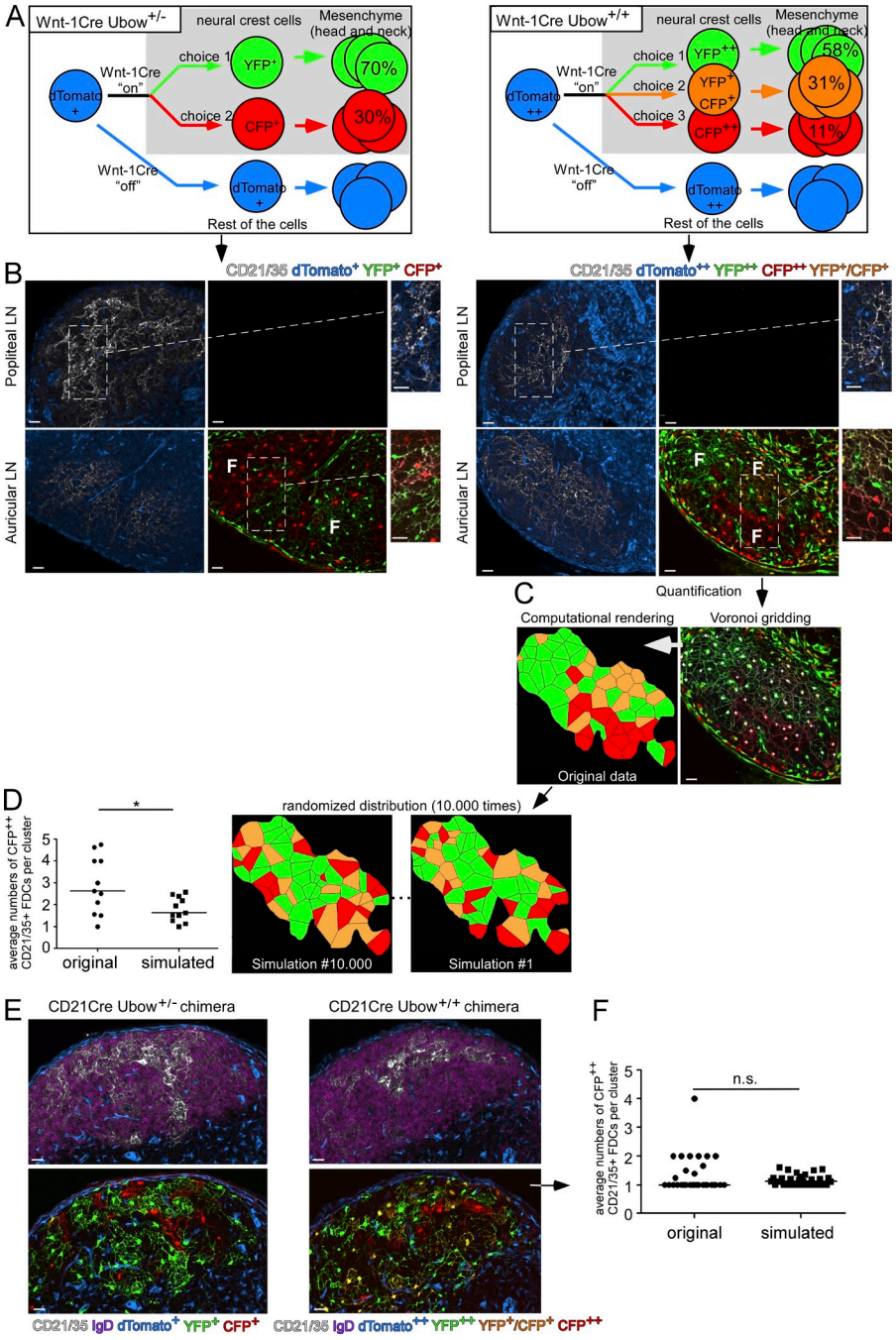

Figure 1. Tracking the ontogeny of FDCs. (A) Schematic showing that in Wnt-1Cre Ubow$^{+/-}$ and $^{+/+}$ mice, neural crest–derived head and neck mesenchymal cells stochastically express YFP or CFP at different ratios while the rest of the cells, including all hematopoietic cells, express dTomato (Ghigo et al., 2013). (B) Auricular and popliteal LN sections from nonirradiated Wnt-1Cre Ubow$^{+/-}$ and $^{+/+}$ mice were stained for CD21/35 expression and analyzed by confocal microscopy. F indicates monocolored foci of FDCs. Insets display high-magnification views of FDCs. (C) All confocal pictures from the auricular/cervical LNs of Wnt-1Cre Ubow$^{+/+}$ mice were processed to generate Voronoi tessellated pictures (see Materials and methods and Fig. S1) amenable to computational simulation. (D) The mean numbers of the rarest colored CD21/35^{+} FDCs (i.e., CFP^{++} FDCs) per CFP^{++} cluster were then compared with Monte Carlo–simulated pictures in which the same colored FDC populations were randomly distributed within the same region of interest (2 simulations displayed out of 10,000). Horizontal bar = median. Each dot represents one follicle. (E) CD21Cre Ubow$^{+/-}$ and $^{+/+}$ mice were irradiated and reconstituted with WT BM cells to generate chimeric mice in which B cell follicles would be composed of colored FDCs and nonfluorescent B cells. 8 wk later, their peripheral LNs were sectioned, stained for CD21/35 and IgD expression, and imaged by confocal microscopy. (F) Quantification of CFP^{++} CD21/35^{+} FDC clustering index in the follicles of CD21Cre Ubow$^{+/+}$ chimera. Horizontal bar = median. Each dot represents one follicle. In D and F, a two-tailed Student's *t* test was used to determine significance. *, $P < 0.05$. n.s. = nonsignificant. Bars, 25m. Data are representative of 4 different experiments (2 mice per experiment, at least 4 analyzed LNs per mouse).

Altogether, these data brought strong evidence that LN FDC network development involves a local and massive proliferation of either FDCs or unknown mesenchymal FDC progenitors.

We further investigated the mechanisms underlying the formation of FDCs during primary follicle development. The association of FDC clusters observed in the upper LNs of Wnt-1Cre^{+} Ubow mice may result from the proliferation of progenitors before their differentiation into FDCs or from the proliferation of differentiated FDCs. To assess the contribution of mature FDC proliferation, we took advantage of CD21Cre mice. In LNs, two stromal subsets express CD21 or originate from cells that expressed this gene: FDCs and the recently described versatile stromal cells (VSCs) that support expansion of inflamed B cell follicles at the T/B interface area (Mionnet et al., 2013). As Cre is expressed by mature radioresistant FDCs and VSCs as well as by radiosensitive B cells (Takahashi et al., 1997; Mionnet et al., 2013), we irradiated CD21Cre Ubow$^{+/-}$ (or $^{+/+}$) mice and reconstituted them with WT (WT = nonfluorescent) BM cells to generate chimeric mice with fluorescent FDCs/VSCs and WT B cells. 8 wk later, peripheral LN sections from CD21Cre Ubow chimeras were stained for CD21/35 expression and analyzed by

confocal microscopy. Although all analyzed LNs displayed CFP and YFP expressing CD21/35$^+$ FDCs, these cells did not assemble into monocolored clusters and were randomly distributed throughout B cell follicles (Fig. 1, E and F). Similar results were obtained in CD21Cre Ubow$^{+/-}$ devoid of B cells (μMt) reconstituted with nonfluorescent mature B cells, ruling out the possibility that the irradiation regimen altered the ability of mature FDCs to proliferate (unpublished data). These experiments suggest that mature FDC or VSC proliferation is not involved in follicular development and rather point to a model in which LN FDCs originate from the clonal proliferation of rare non-FDC, tissue-resident mesenchymal progenitors.

Accumulation of FDCs in reactive LNs does not rely on the recruitment or the proliferation of FDCs

One of the key functions of FDCs is the organization of GC structures devoted to the development and maturation of B cell responses (MacLennan, 1994; Allen et al., 2007; Wang et al., 2011; Victora and Nussenzweig, 2012). GCs contain enlarged FDC networks of unknown origin (Allen et al., 2004, 2007; Allen and Cyster, 2008). A previous report indicated that during carcinogenesis, at least 20% of carcinoma-associated fibroblasts originate from BM-derived mesenchymal stem cells (Quante et al., 2011). We thus sought to determine whether FDCs in inflamed follicles also arose from the recruitment of BM-derived stromal cells or derived from the proliferation of resident FDCs. We first addressed the contribution of blood-derived FDC precursors. To this aim, we took advantage of Wnt-1Cre Ubow mice in which cervical and auricular LNs display CFP$^+$ and YFP$^+$ FDCs at steady-state (Fig. 1 B). We injected an emulsion of OVA in CFA in the ears and rear footpads of these mice and analyzed the FDC networks of their auricular and popliteal LNs 3 wk later. As expected, confocal microscopy indicated that the FDC networks of inflamed auricular LNs contained CFP$^+$ and YFP$^+$ FDCs (Fig. 2 A, left). However, none of the inflamed popliteal LNs displayed CFP$^+$ or YFP$^+$ FDCs, ruling out the possibility that circulating neural crest–derived mesenchymal precursors migrated into reactive LNs and generated FDCs (Fig. 2 A, right). To exclude the implication of other circulating mesenchymal derived progenitors, we set up parabiotic pairs of mice consisting of CD21Cre Ubow$^{+/-}$ μMT mice surgically attached to WT counterparts (Kitamura et al., 1991; Waskow, 2010; Fig. 2 B). In such parabionts, both mice share their blood circulation and thus a common probability to recruit a putative circulating FDC precursor. If such precursor arises from the CD21Cre Ubow$^{+/-}$ μMT partner, it should generate CFP$^+$ or YFP$^+$ mature CD21/35$^+$ FDCs upon its engraftment in the reactive LNs of the WT mouse. 3 mo after the surgery, the WT partners (all displaying full chimerism) were injected with CFA/OVA in their rear footpads. 3 wk later, their inflamed popliteal LNs were analyzed by confocal microscopy for the presence of CFP$^+$ or YFP$^+$ CD21/35$^+$ FDCs. Analysis indicated that CFP$^+$ or YFP$^+$ CD21/35$^+$ FDCs were absent in the inflamed follicles of the WT parabionts (Fig. 2 B) while all the follicles of CD21Cre Ubow$^{+/-}$ μMT partners displayed YFP or CFP FDC networks as a result of WT B cell seeding. Altogether, our results rule out the possibility that reactive FDC networks incorporate putative blood-derived FDCs.

We next investigated the contribution of local FDC and VSC proliferation to the development of reactive follicles. To this aim, CD21Cre Ubow$^{+/-}$ and $^{+/+}$ chimeras were injected with CFA/OVA and their draining LNs were analyzed by confocal microscopy 3 wk later. As the LN FDCs of these mice did not assemble into monocolored clusters at steady-state (Fig. 1 E), any appearance of such clusters in inflamed LNs would reveal the proliferation of mature FDCs or VSCs. Confocal pictures and quantification indicated that FDCs were randomly distributed within reactive follicles (Fig. 2, C and D), suggesting that FDC and VSC proliferation does not constitute a major source of FDCs in reactive follicles.

FDC progenitors proliferate and differentiate in reactive follicles

As FDCs were not recruited from the circulation and did not divide in reactive follicles, we reasoned that they could originate from the local proliferation of CD21/35-negative FDC progenitors. According to this scenario, these progenitors would divide and give rise to daughter cells that would randomly acquire CFP or YFP expression upon CD21 expression. This postmitotic acquisition of colors would thus explain the absence of monocolored FDC foci observed in CD21Cre Ubow inflamed LNs. To unravel such a CD21/35$^-$ progenitor, we developed a third fate mapping system in which all stromal cells could undergo combinatorial recombination of the Ubow construct. RAG-2$^{o/o}$ Ubow$^{+/+}$ mice were crossed to tamoxifen Cre-inducible Ubiquitin-Cre-ERT2 mice (Hayashi and McMahon, 2002; hereafter referred to as Ubow-CreERT2), irradiated, and reconstituted with WT BM cells. Reconstituted chimeras were treated with tamoxifen for 3 consecutive days and then maintained under a tamoxifen-free regimen for 1 wk to eliminate any remaining tamoxifen activity (Fig. S3). Mice were then injected with an emulsion of CFA/OVA in their ears and rear footpads (left side only). Inflamed (left) and control (right) auricular and popliteal LNs were harvested 3 wk later and stained for CD21/35 expression (Fig. 3). We reasoned that if CD21/35$^-$ FDC progenitors proliferated during that period, they should have generated foci of colored FDCs around them and thus unraveled their own localization in the follicle. Confocal analysis revealed that very few sparse FDCs in control follicles underwent recombination (Fig. 3 A). On the contrary, inflamed follicles were populated by nonrandomly distributed monocolored columnar foci of FDCs often connected to the subcapsular sinus (SCS; Fig. 3, B and C), indicative of local cell proliferation.

As such columns and clusters were absent in the inflamed LNs of CD21Cre Ubow chimeric mice, we concluded that they should have been generated by FDC progenitors before their differentiation into mature CD21/35-expressing FDCs. We thus undertook the identification of these progenitors.

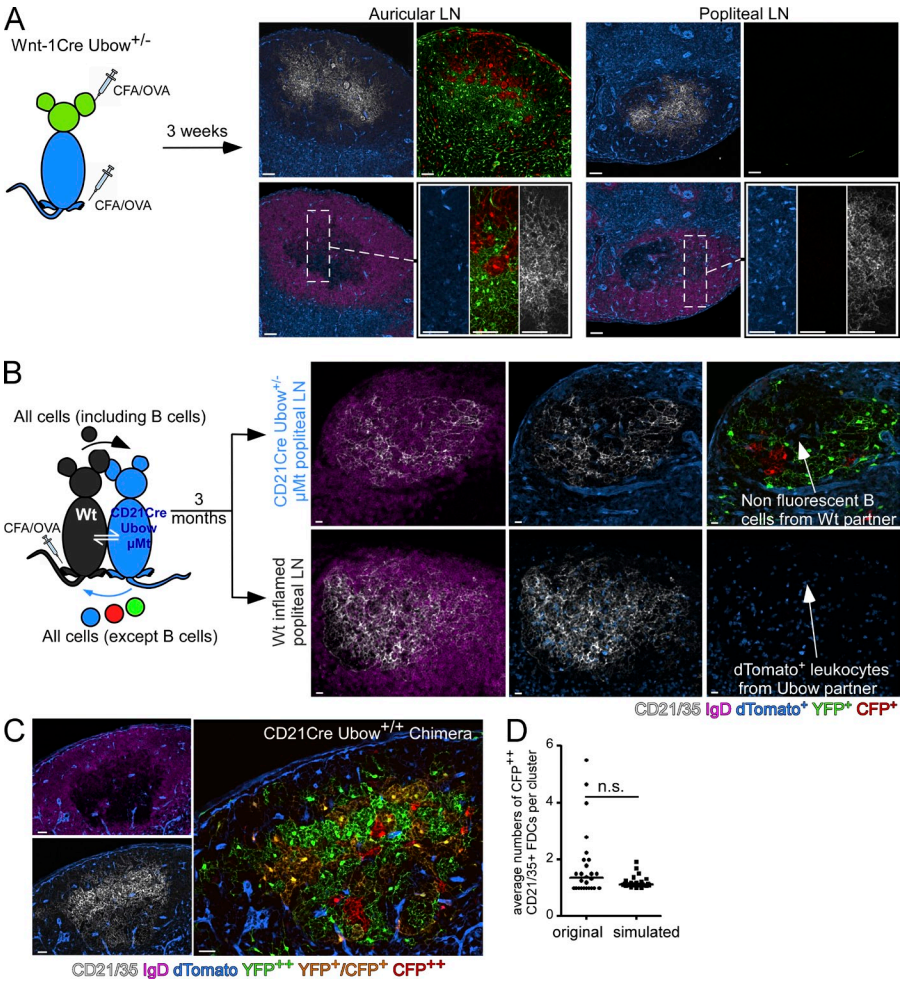

Figure 2. Reactive FDCs do not originate from circulating progenitors. (A) Wnt-1Cre Ubow$^{+/-}$ mice were injected with an emulsion of CFA/OVA in their ears and rear footpads. 3 wk later, inflamed auricular and popliteal draining LNs were sectioned, stained for CD21/35 and IgD expression, and analyzed by confocal microscopy. Insets display high-magnification views of FDCs. Data are representative of 3 different experiments (2 mice per experiment, 4 analyzed LNs per mouse). (B) WT mice were joined surgically with naive CD21Cre Ubow$^{+/-}$ µMt mice to create parabiotic mice. 3 mo later, when full chimerism was achieved, the WT partner was injected with CFA/OVA in its rear footpads. 3 wk later, popliteal LNs of both mice were sectioned, stained for CD21/35 and IgD expression, and the presence of colored FDCs in their LNs was analyzed by confocal microscopy. The development of mature FDC networks in the µMt mouse combined to the appearance of dTomato^{+} leukocytes in the WT partner indicates successful chimerism. Data are representative of 3 different experiments (2 mice per experiment). (C) CD21Cre Ubow$^{+/+}$ chimeras were injected with an emulsion of CFA/OVA in their ears and rear footpads. 3 wk later, inflamed draining LNs were sectioned, stained for CD21/35, and IgD expression and analyzed by confocal microscopy. (D) Quantification of CFP^{++} CD21/35^{+} FDC clustering index in the follicles of CD21Cre Ubow$^{+/+}$ chimera. Horizontal bar = median. Data are representative of 4 different experiments (2 mice per experiment, 4 LNs analyzed per mouse). Each dot represents one follicle. In A and D, a two-tailed Student's *t* test was used to determine significance. n.s = nonsignificant. Bars, 25 µm.

MRCs act as FDC progenitors during B cell follicle development and remodeling

The outer edge of follicles is populated by MRCs, a poorly defined stromal cell population thought to descend from lymphoid tissue organizer (LTo) cells (Katakai et al., 2008, 2012). MRCs express receptor activator of NF-κB ligand (RANK-L) and mucosal vascular addressin cell adhesion molecule 1 (MAdCam-1), and construct a reticulum of stromal cells between the SCS and the underlying FDC network. The unique location of MRCs combined with the arrangement of FDCs in clusters connected to the SCS in the primary follicles of Wnt-1Cre Ubow mice and in the GCs of immunized Ubow-CreERT2 mice raised the interesting possibility that MRCs could be the precursors of LN FDCs during ontogeny and inflammation (Figs. 1 B and 3 B).

To test this hypothesis, we first stained LN sections harvested from resting Wnt-1Cre Ubow$^{+/+}$ mice and inflamed Ubow-CreERT2 chimeras for RANK-L expression (Fig. 3, D and F; and Video 1). Confocal pictures indicated that in both types of mice, monocolored columns of stromal cells contained nonrandomly associated RANK-L^{hi} CD21/35^{-} MRCs juxtaposed to RANK-L^{-} CD21/35^{+} mature FDCs, suggesting that MRCs and FDCs derived from a common progenitor and/or that MRCs gave rise to the underlying FDCs (Fig. 3 E and Fig. S2).

To address the affiliation of MRCs and FDCs, we used another feature of the Ubow mouse. In the Ubow mouse, all cells express dTomato and upon Cre action, cells undergo a single recombination event that triggers YFP or CFP expression. Although Cre genetically switches off the production of dTomato in any Ubow-expressing cell, it does not act on the pool of cytoplasmic dTomato protein that should slowly decrease and eventually wash out (Fig. 4 A). In summary, any Ubow cell that expresses Cre should transiently coexpress dTomato and YFP (or CFP) before acquiring its final color (YFP or CFP). As a proof of principle, we treated Ubow$^{+/-}$ CreERT2 mice with a single dose of tamoxifen and followed the colors of their blood lymphocytes over time (Fig. 4 B).

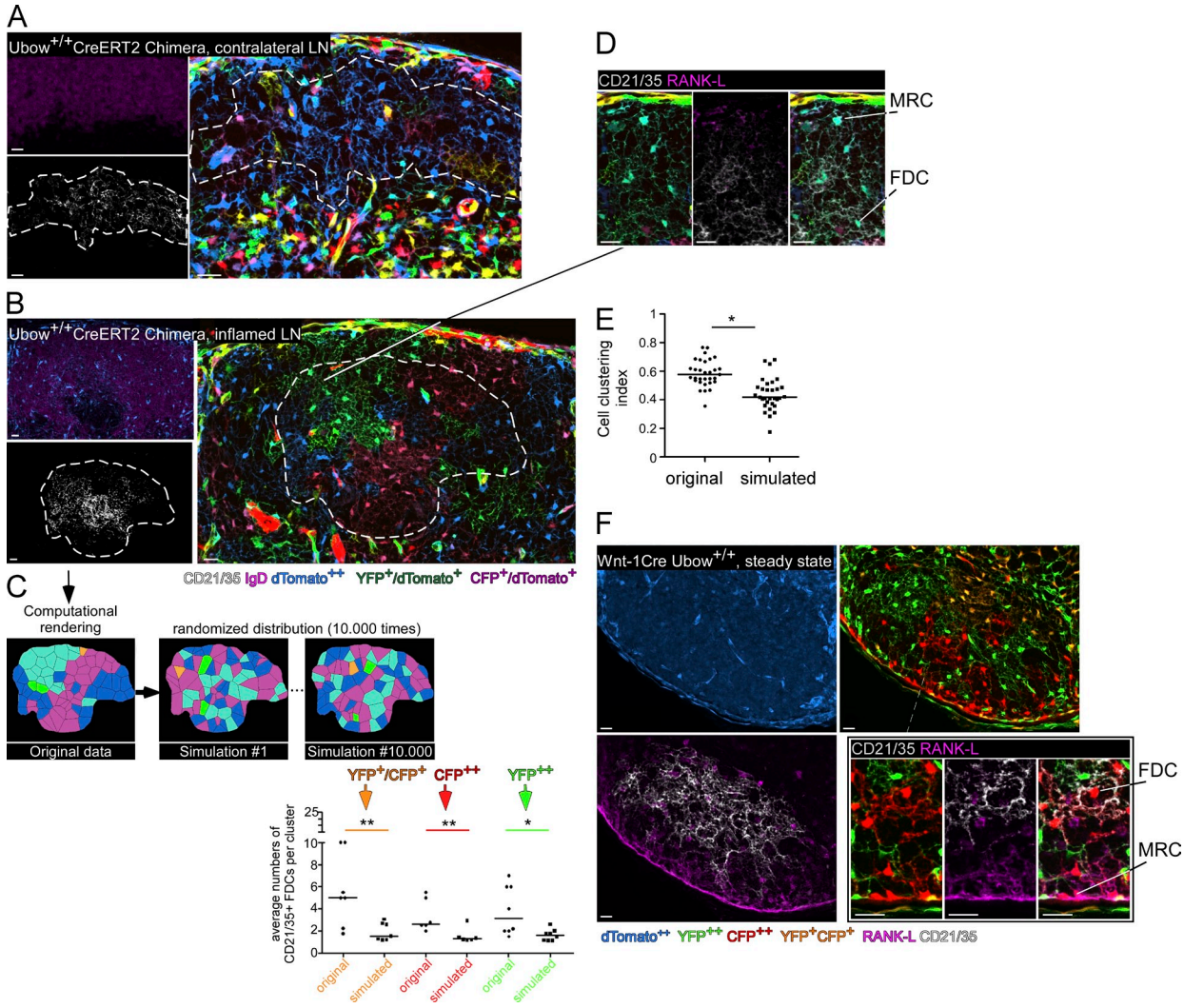

Figure 3. Lineage tracing of FDC progenitors. Ubow^{++}-CreERT2 mice were irradiated and reconstituted with WT BM cells to generate chimeric mice with fluorescent stromal cells and nonfluorescent hematopoietic cells. Reconstituted chimeras were treated with tamoxifen, maintained under tamoxifen-free regimen during 1 wk, and injected with an emulsion of CFA/OVA in their ears and rear footpads (left side only). 3 wk later, inflamed popliteal and auricular LNs (B and C) and contralateral LNs (A) were sectioned, stained for CD21/35 (dashed line) and IgD (A and B) or RANK-L (D) expression, and analyzed by confocal microscopy. (C) Quantification of CFP^{++} YFP^{++} CFP^{+}YFP^{+} CD21/35^{+} FDC clustering index. Horizontal bar = median. Data are representative of 3 different experiments (2 mice per experiment, 4 LNs analyzed per mouse). Each dot represents one follicle. (E) Comparison of MRC/FDC cluster formation as measured by the clustering index (see Materials and methods section and Fig. S2 for details) in original and simulated data. Each dot represents the cell clustering index of a cell cluster composed of MRCs and FDCs sharing a similar color, in original and Monte Carlo–simulated data. See also Video 1. (F) Auricular/cervical LN sections from Wnt-1Cre Ubow$^{+/+}$ mice were stained for CD21/35 and RANK-L expression and analyzed by confocal microscopy. Insets in D and F represent magnified views of juxtaposed MRCs and FDCs sharing a similar color. Data are representative of 3 different experiments (2 mice per experiment, 2 LNs analyzed per mouse). In E and C, a two-tailed Student's *t* test was used to determine significance. *, $P < 0.08$; **, $P < 0.01$. n.s. = nonsignificant. Bars, 25 µm.

At day 0, all lymphocytes exclusively expressed dTomato. 1 d later, dTomato^{+} lymphocytes started to express CFP or YFP. During the subsequent days, CFP and YFP expression progressively increased in dTomato-expressing cells. The first single, bright YFP^{+} (or CFP^{+}) cells negative for dTomato expression appeared at day 6 while the remaining transitional cells gradually lost dTomato in an asynchronous manner, probably reflecting a gradual tamoxifen-induced recombination and intrinsic differences in fluorescent protein degradation (Fig. S3). Altogether, these results indicate that, upon Cre activation, any Ubow cell goes through a transitional step characterized by the coexpression of dTomato and CFP or YFP.

Having validated the Ubow mouse as a powerful tool to track transitional cells, we used CD21Cre Ubow mice to determine the putative filiation of MRCs and FDCs during ontogeny and inflammation. If MRCs were FDC progenitors, they should proceed through sequential maturation steps. Upon differentiation, MRCs should evolve from their primordial

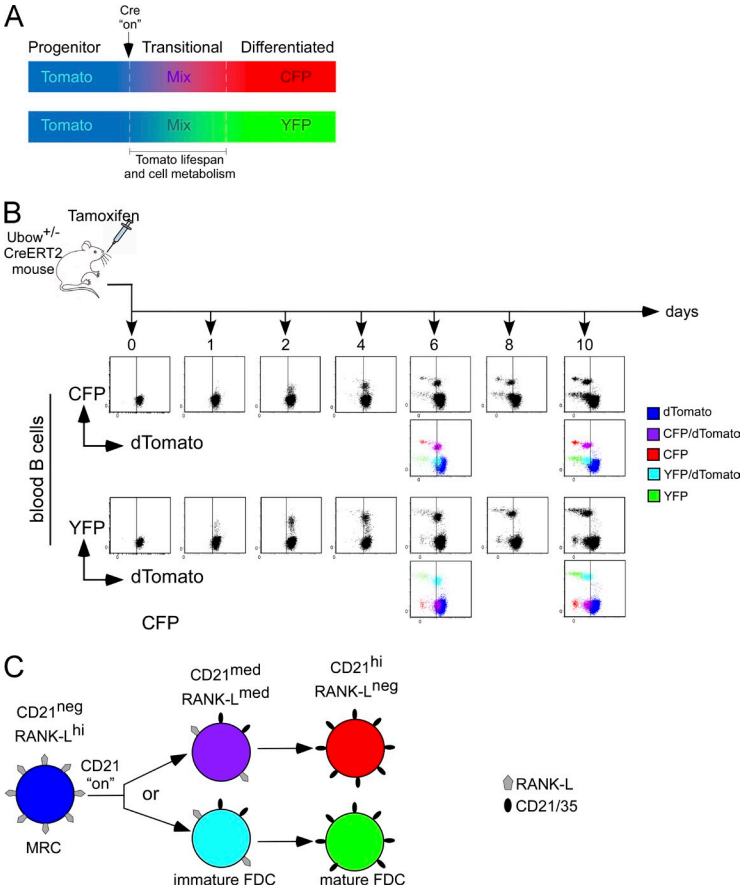

Figure 4. Cellular filiation in the Ubow mouse. (A) Schematic describing that when Ubow cells express Cre, they simultaneously lose dTomato and acquire CFP or YFP expression. Applied to a precursor/product relationship and in combination with the proper Cre reporter strain, this system unravels the transitional stage between progenitors and their differentiated cells. (B) Non-chimeric Ubow$^{+/-}$-CreERT2 mice were injected with a single dose of tamoxifen. Mice were bled every day and the relative proportion of CFP-, YFP-, and dTomato-expressing B220^{+} B cells were assessed by flow cytometry (same results were observed in CD3^{+} T cells). Data are representative of 3 different mice from 3 different experiments. (C) Schematic showing the expected phenotypes and colors of MRCs (RANK-L^{hi} CD21^{neg}) and immature (RANK-L^{med} CD21^{med}) and mature FDCs (RANK-L^{neg} CD21^{hi}) in CD21Cre Ubow mice according to the model in which MRCs give rise to FDCs.

phenotype (CD21/35^{-} RANK-L^{hi} dTomato^{hi} CFP/YFP^{neg}), then adopt a transitional stage (CD21/35^{+} RANK-L^{med} dTomato^{med} CFP/YFP^{med}), before acquiring the mature FDC status (CD21/35^{+} RANK-L^{neg} dTomato^{neg} CFP/YFP^{hi}; Fig. 4 C).

As LN MRCs reside below the SCS, we analyzed the outer follicle of inflamed LNs harvested from CD21Cre Ubow$^{+/+}$ chimeras. Confocal pictures indicated that CD21/35^{-} RANK-L^{hi} dTomato^{+} CFP^{neg}YFP^{neg} MRCs formed a cellular layer below the SCS of reactive follicles (Fig. 5 A). Interestingly, a discrete population of maturing CD21/35^{+} RANK-L^{med} dTomato^{med} CFP^{med} (or YFP^{med}) FDCs was immediately juxtaposed to this MRC layer and contiguous to the more central population of mature CD21/35^{+} RANK-L^{neg} dTomato^{neg} CFP^{hi} (or YFP^{hi}) FDCs. As LN FDCs cannot be efficiently isolated from nonirradiated LNs, we next quantified the colors and numbers of MRCs and transitional and mature FDCs on tissue sections. The great majority of CD21/35^{-} RANK-L^{+} MRCs expressed dTomato in the absence of YFP or CFP while almost all mature CD21/35^{+} RANK-L^{-} FDCs expressed YFP or CFP in absence of dTomato (Fig. 5 C). Interestingly, 77% of CD21/35^{+} RANK-L^{+} cells (172 out of 223 cells) coexpressed dTomato and YFP or CFP, confirming their transitional stage between MRCs and mature FDCs. In addition, these transitional cells represented 1.9% of all RANK-L^{+} cells (30 out of 1,514 cells) in control LNs while they represented 16.6% of all RANK-L^{+} cells (323 out of 1,935 cells) in inflamed LNs, suggesting that such transition was increased in reactive follicles. To rule out the contribution of an unknown follicular cell type to the generation of FDCs, we also analyzed the colors of all RANK-L^{-} CD21/35^{-} fluorescent cells present in the follicles of these mice. These data show that the majority of these cells expressed dTomato while very few of them coexpressed dTomato and YFP (or CFP), confirming that the transitional phenotype was almost exclusively observed in MRCs and FDCs. Further analysis indicated that dTomato^{+} RANK-L^{+} MRCs expressed CXCL13 but did not display the pre-FDC markers NG2 and Mfge-8 (Krautler et al., 2012; not depicted), supporting the recent evidence that splenic and LN FDC progenitors are of different origins (Castagnaro et al., 2013). These results indicate that MRCs give rise to FDCs during inflammation-induced remodeling of B cell follicles.

We next analyzed the ability of MRCs to generate FDCs during follicle development. To this aim, we adoptively transferred WT B cells in nonirradiated CD21Cre Ubow$^{+/-}$ μMt mice devoid of B cells and FDCs and determined the location, phenotype, and colors of MRCs and FDCs 1 wk later by confocal microscopy (Fig. 5, B and C). As expected, no FDCs and no transitional cells were observed in mice that were not injected with B cells (unpublished data) while LN B cell follicles of mice injected with B cells displayed MRCs, FDCs, and transitional cells. Transitional

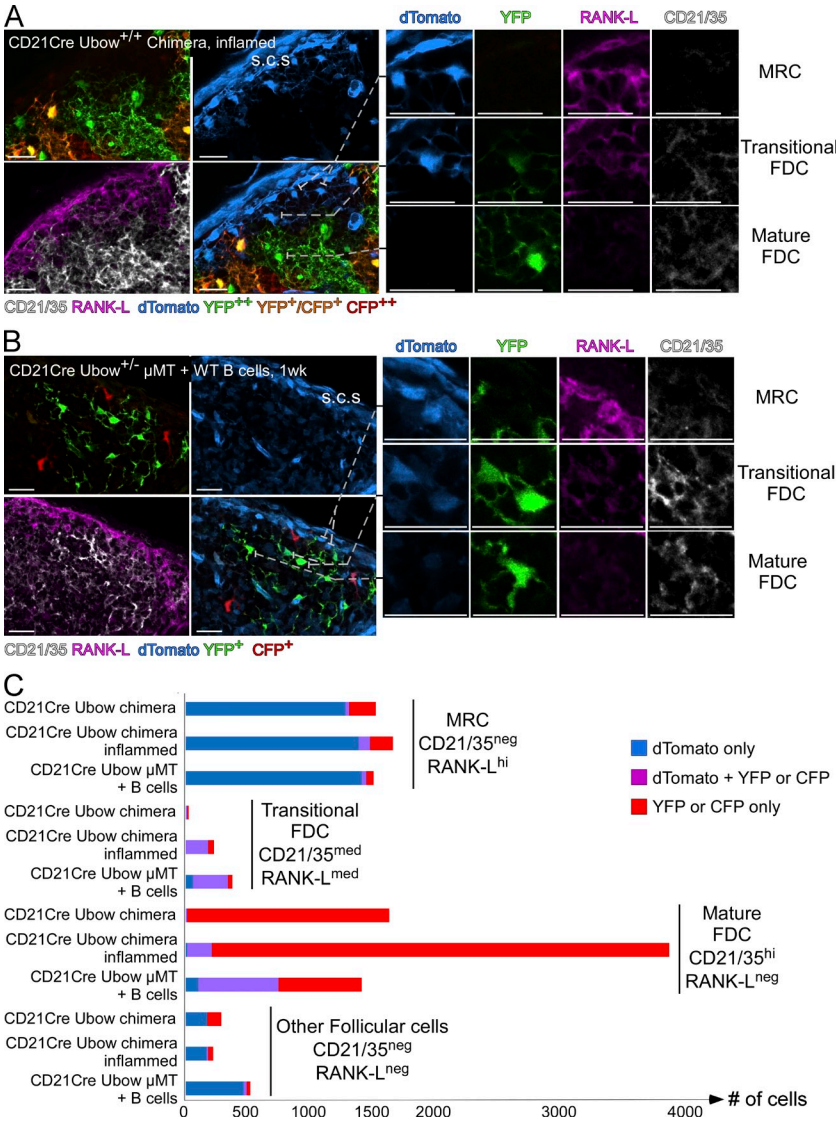

Figure 5. Tracking CD21⁻ FDC progenitors. (A) CD21Cre Ubow$^{+/+}$ chimeras were injected with an emulsion of CFA/OVA in their ears and rear footpads to trigger FDC remodeling in their draining LNs. 3 wk later, inflamed draining LNs were sectioned and stained for CD21/35 and RANK-L expression. (B) CD21Cre Ubow$^{+/-}$ µMT mice were adoptively transferred with 6×10^7 WT polyclonal B cells to trigger FDC development. 1 wk later, peripheral LNs were sectioned and stained for CD21/35 and RANK-L expression. In A and B, data are representative of 3 different experiments (3 mice per experiment, 4 LNs analyzed per mouse). Insets display high-magnification views of MRC and transitional and mature FDCs. (C) Confocal pictures acquired in all the experiments described in A and B were used to determine the colors and absolute numbers of MRCs, transitional and mature FDCs, and other cells present in B cell follicles. Bars, 25 µm.

cells represented 20% of all RANK-L$^+$ cells (362 out of 1,460 cells) and expressed dTomato together with YFP or CFP, demonstrating that these cells recently switched on the *Cr2/CD21* promoter. Interestingly, 45% of CD21/35$^+$ RANK-L$^-$ FDCs (619 out of 1,370 cells) coexpressed dTomato and YFP (or CFP) 7 d after B cell transfer. Because at least 6 d was required to observe a full switch of colors in Ubow cells undergoing Cre-mediated recombination (Fig. 4 B), these transitional FDCs could represent newly differentiated cells that have not yet acquired their final color. To test this hypothesis, we analyzed the colors of FDCs in the LNs of CD21Cre Ubow$^{+/-}$ µMt adoptively transferred with B cells 9 d before. As expected, the proportion of transitional CD21/35$^+$ FDCs expressing both dTomato and YFP (or CFP) dropped to 12% (42 out of 350 CD21/35$^+$ FDCs; not depicted) in these LNs, suggesting that these FDCs represent newly differentiated cells. Although we cannot rule out a contribution of other cell types to the generation of FDCs, our results strongly suggest that MRCs give rise to FDCs during B cell follicle development and inflammation-induced remodeling.

Marginal reticular cells proliferate before differentiating into FDCs

Although the data described above suggest that MRCs generate FDCs during B cell follicle development and inflammation-induced remodeling, the absence of FDC clusters in the LNs of CD21Cre Ubow chimeras indicates that this process does not rely on FDC proliferation. Thus, the presence of monocolored columns and clusters of FDCs in the resting LNs of Wnt-1Cre Ubow mice, as well as in the inflamed LNs of Ubow-CreERT2 chimeric mice, strongly favors a model in which MRCs proliferate before differentiating into FDCs. To test this hypothesis, we investigated the capacity of MRCs and FDCs to incorporate 5-ethynyl-2′-deoxyuridine (EdU), a thymidine analogue, in inflamed and developing LNs.

WT mice were immunized s.c. with CFA/OVA to induce FDC network remodeling in their inflamed LNs. Animals were injected with EdU 4, 9, and 20 d after immunization, and 1 d later, LN cell suspensions were stained for EdU, CD21/35, CD45, CD31, gp38, and MAdCam-1 expression and analyzed by flow cytometry (Fig. 6), as previously described (Fletcher et al., 2011). The percentage of EdU$^+$ MRCs (CD21/35$^-$ CD45$^-$ CD31$^-$ gp38$^+$ MAdCam-1$^+$) and EdU$^+$ FDCs (CD21/35$^+$ CD45$^-$ CD31$^-$ gp38$^+$) was then determined for each time point (Fig. 6 A). Flow cytometry analysis revealed a burst of MRC proliferation at day 5 (13.4% of EdU$^+$ MRCs vs. 1.9% in control LNs), followed by a progressive decrease of MRC proliferation over time (5.9% of EdU$^+$ MRCs at day 10 and 5.2% at day 21; Fig. 6 B). As an alternative approach, we used confocal imaging to quantify the percentage of EdU$^+$ MRCs and EdU$^+$ FDCs in the LNs of CD21Cre Ubow chimeric mice subjected to the same experimental protocol. As depicted in Fig. 6 C, in situ quantification indicated that 9.7% (56 out of 574) MRCs and 1.5% (5 out of 329) FDCs incorporated EdU at day 5 after immunization. Altogether, our results demonstrate that MRCs actively proliferate in inflamed LNs.

A small increase in the percentage of EdU$^+$ FDCs was also observed in inflamed LNs, suggesting that FDCs were also able to proliferate to a lesser extent or that such EdU$^+$ FDCs represented recent postmitotic transitional cells that inherited EdU from proliferating MRCs. To explore this hypothesis, we designed a BrdU pulse-chase experiment. If inflammation triggers the differentiation of proliferating MRCs into nonproliferating FDCs, the frequency of proliferating BrdU-labeled MRCs should decrease over time as a result of their progressive incorporation in the pool of FDCs. This phenomenon should thus be accompanied by an increase in the frequency of BrdU$^+$ FDCs that would have inherited BrdU from these pulse-labeled MRCs. WT mice were injected s.c. with CFA/OVA in ears and footpads, followed by BrdU injection (i.p) on day 4 when MRCs extensively proliferate. This pulse of BrdU was followed by a chase period of 1 and 3 d (Fig. 6 D). At the end of the chase period, the percentage of BrdU-labeled MRCs and FDCs was determined by flow cytometry. These data indicated that the frequency of BrdU$^+$ MRCs progressively decreased between day 1 and 3 (10.2% of BrdU$^+$ MRCs at day 1 vs. 7.8% at day 3) while the percentage of BrdU$^+$ FDCs simultaneously increased (4.8% of BrdU$^+$ FDCs at day 1 vs. 11.5% at day 3). As FDCs proliferated poorly and did not form monocolored clusters in the inflamed LNs of CD21Cre Ubow mice (Fig. 2 C), the progressive increase of BrdU-labeled FDCs in this pulse-chase experiment suggests that MRCs proliferate before differentiating into FDCs in inflamed LNs.

Next, we assessed the contribution of MRC proliferation to the development of LN FDCs. The SLOs of RAG-2$^{o/o}$ mice lack FDC networks that can be reconstituted by an adoptive transfer of B cells (Fu et al., 1998). We adoptively transferred 6 × 10^7 WT B cells to RAG-2$^{o/o}$ mice, and 1 wk later, when many MRCs were maturing into FDCs (Fig. 5), mice were injected i.p with EdU. 1 d later, the percentage of

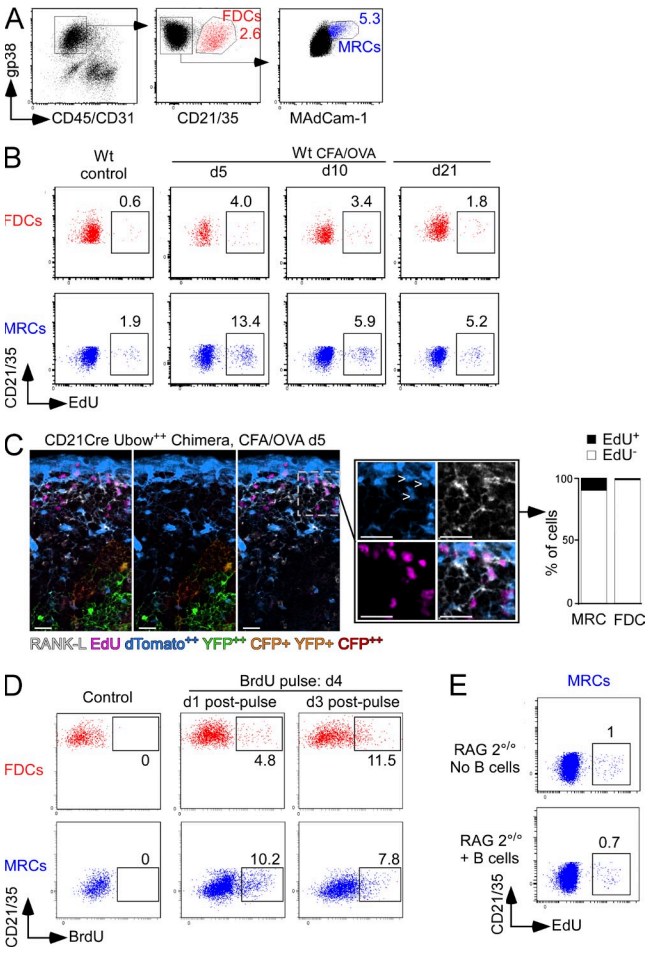

Figure 6. MRCs proliferate during inflammation. (A) Flow cytometry gating strategies used to identify MRCs (gp38$^+$ MAdCam-1$^+$ CD45$^-$ CD31$^-$ CD21/35$^-$) and FDCs (gp38$^+$ CD45$^-$ CD31$^-$ CD21/35$^+$) in LN cellular suspensions. WT mice (B) and CD21Cre Ubow^{++} chimeras (C) were subcutaneously injected or not with an emulsion of CFA/OVA. (B) 4, 9, or 20 d later, mice received a single i.p. injection of EdU to label proliferating cells. 1 d later, the percentages of EdU$^+$ MRCs and EdU$^+$ FDCs present in the peripheral inflamed LNs of WT mice were analyzed by flow cytometry. (C) The percentage of EdU$^+$ MRCs (arrowheads) and EdU$^+$ FDCs was determined at day 5 by confocal imaging in the inflamed LNs of CD21Cre Ubow^{++} chimeras. Insets display high-magnification views of EdU$^+$ MRCs. Bars, 25 µm. Data are representative of 3 experiments (at least 4 mice pooled per group in B and 2 LNs analyzed per mouse in C). (D) WT mice were injected s.c. with CFA/OVA in ears and footpads, followed by BrdU injection (i.p) on day 4. This pulse of BrdU was followed by a chase period of 1 and 3 d. At the end of the chase period, the percentage of BrdU-labeled MRCs and FDCs was determined by flow cytometry. Data are representative of 3 different experiments (5 mice pooled per group). (E) RAG-2$^{o/o}$ mice were adoptively transferred or not with 6 × 10^7 WT polyclonal B cells. 1 wk later, mice received a single injection of EdU. The proportion of EdU$^+$ cells among the MRCs and FDCs of peripheral LNs were analyzed one day later by flow cytometry. At this stage, no mature FDCs could be recovered from the LNs of both types of mice. Data are representative of 3 different experiments (5 mice pooled per group).

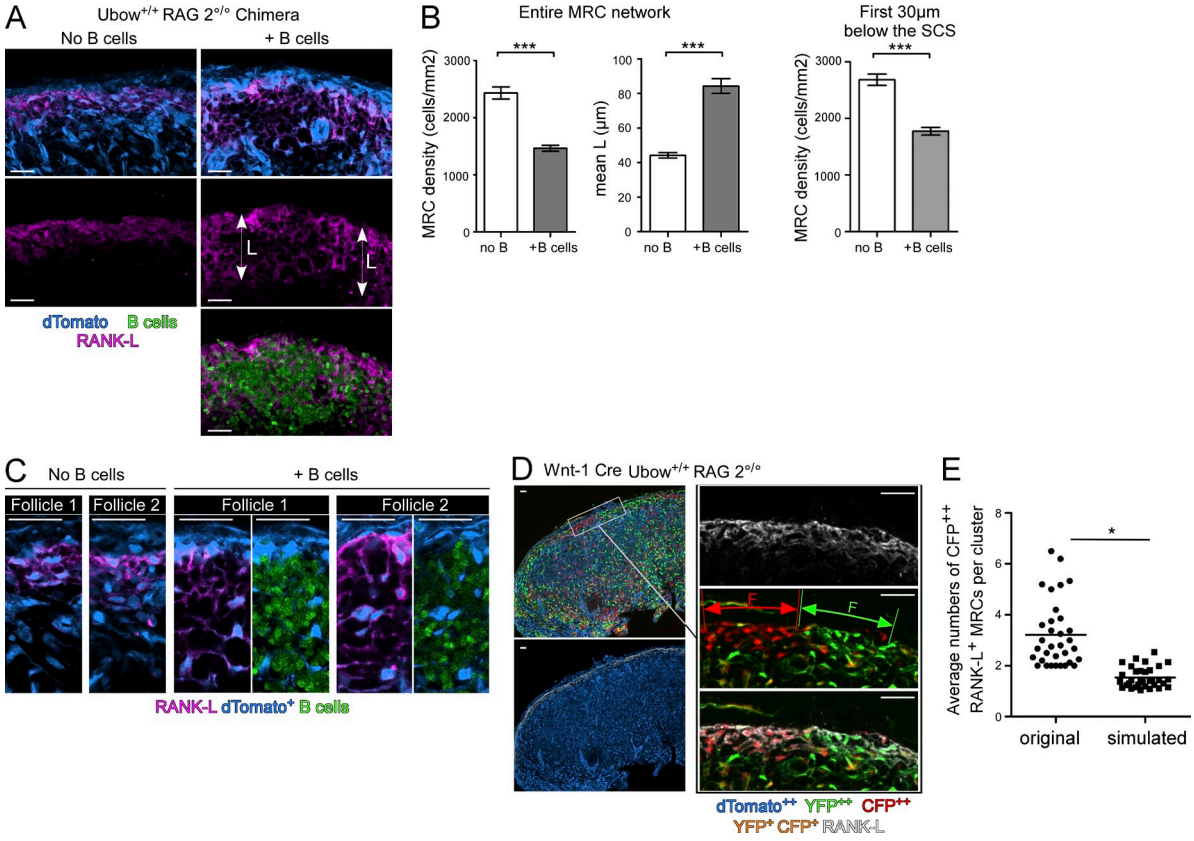

Figure 7. Postmitotic LN MRC network is remodeled upon initial B cell colonization. (A) RAG-2°/° Ubow mice were irradiated and reconstituted with RAG-2°/° nonfluorescent BM cells to generate chimeric mice with dTomato-expressing stromal cells. Reconstituted chimeras were adoptively transferred or not with 6×10^7 CMFDA-labeled polyclonal WT B cells to trigger FDC development in recipient LNs. 1 d later, peripheral LNs were sectioned, stained for RANK-L expression, and analyzed by confocal microscopy. L displays the width of the MRC network based on RANK-L staining. (B) The number of RANK-L$^+$ dTomato$^+$ cellular bodies was manually counted on tissue sections and used to calculate the density of the dTomato$^+$ RANK-L$^+$ MRC network in the two types of LNs, either in its globality (left) or in the first 30 µm below the SCS (right). Data are representative of 3 different experiments (2 mice per experiment, 6 LNs analyzed per mouse). (C) Representative high-magnification views of the MRC network present in the 2 types of LNs. (D) Auricular/cervical LN sections from Wnt-1Cre Ubow$^{+/+}$ RAG-2°/° mice were stained for RANK-L expression and analyzed by confocal microscopy. Note the presence of MRCs Foci (F) in the SCS of these LNs devoid of B cells. Insets on the right display high-magnification views of MRC clusters. (E) Quantification of CFP^{++} RANK-L$^+$ MRC clustering index in the auricular/cervical LNs of Wnt-1Cre Ubow$^{+/+}$ RAG-2°/° mice. A two-tailed Student's *t* test was used to determine significance. *, $P < 0.05$; ***, $P < 0.001$. Bar = median. Data are representative of 5 individual mice (4 LNs analyzed per mouse) obtained in 2 independent experiments. Each dot represents one follicle. Bars, 25 µm.

EdU-labeled MRCs was analyzed by flow cytometry. Surprisingly, the percentage of proliferating (EdU$^+$) MRCs in RAG-2°/° mice after B cell transfers was similar to that observed in mice that did not receive B cells (Fig. 6 E), suggesting that B cells did not trigger MRC proliferation but rather converted them into FDCs. To investigate this possibility, we determined the impact of B cells on the MRC network 24 h after their adoptive transfer, long before the appearance of the first mature FDCs (unpublished data). To this aim, we generated mice in which all stromal cells could be independently visualized in tissue section. RAG-2°/° Ubow mice were irradiated and reconstituted with nonfluorescent RAG-2°/° BM cells. 8 wk later, chimeric mice were adoptively transferred or not with CMFDA-labeled 6×10^7 B cells. 1 d later, LNs were sectioned, stained for RANK-L expression, and analyzed by confocal microscopy (Fig. 7 A). RANK-L$^+$ dTomato$^+$ MRCs formed a dense meshwork of short radioresistant stromal cells below the SCS of nontransferred mice (Fig. 7, A and C, left; Katakai et al., 2008). In contrast, upon B cell adoptive transfer, MRCs spread deeper in the follicle and harbored many cellular processes (Fig. 7, A and C, right), a morphological feature shared with mature FDCs (Fig. 5). Quantification of RANK-L$^+$ dTomato$^+$ cell bodies and mean width of the MRC territory indicated that B cells lead to the generation of a larger but less dense MRC network, even in the first 30-µm corridor abutting the SCS (Fig. 7 B). Accordingly, the total number of MRC cell bodies was similar in the MRC networks of control and B cell–injected mice, indicating that upon their arrival in the LN, B cells induce a topographic change rather than the proliferation of the preexisting MRC network.

Based on these results, we reasoned that the monocolored clusters of FDCs observed in the upper LNs of adult Wnt-1Cre

Ubow mice resulted from the deployment of MRC clusters generated before B cell colonization. According to this hypothesis, monocolored clusters of MRCs should already be present in the upper LNs of RAG-2$^{-/-}$ Wnt-1Cre Ubow$^{+/+}$ mice. Confocal analysis of the upper LNs of these mice combined with statistical quantification confirmed the existence of clusters of MRCs (Fig. 7, D and E), thus demonstrating that MRC proliferation can precede LN B cell colonization. Altogether, our results point to a model in which B cell colonization induces SCS lining MRC network deployment toward the underlying parenchyma and its subsequent maturation into the FDC network, hence rapidly generating the follicular primary FDC network.

DISCUSSION

FDCs orchestrate the development and maintenance of B cell follicles in SLOs (Allen and Cyster, 2008; Wang et al., 2011). These stromal cells are of mesenchymal origin and develop after birth (Endres et al., 1999; Muñoz-Fernández et al., 2006; Wilke et al., 2010; Krautler et al., 2012). Recent evidence suggests that splenic FDCs originate from pre-FDCs, a subset of ubiquitous PDGFRβ^+ mural cells deriving from a Nkx2-5$^+$ Islet-1$^+$ mesenchymal lineage (Krautler et al., 2012; Castagnaro et al., 2013). As these lineage-tracing experiments demonstrated that LN and Peyer's patch FDCs did not derive from the Nkx2-5$^+$ Islet-1$^+$ mesenchymal lineage, the origin of LN FDCs remained ambiguous. Similarly, the cellular mechanisms underlying the tremendous reshaping of the FDC network occurring during GC development were poorly characterized. Herein, we have used multiple lineage tracing systems to unravel the cellular steps leading to the establishment of LN FDC networks and their subsequent remodeling into reactive follicles. We report that LN FDCs originate from the proliferation and conversion of tissue-resident MRCs. Upon inflammation, neither the proliferation nor the recruitment of FDCs significantly contributed to the expansion of the FDC network. Rather, we demonstrate that tissue-resident MRCs massively proliferate and subsequently differentiate into FDCs, thus providing seminal information on the development of GC reactions.

One key function of the FDC network is to trap and retain Ag in the form of immune complexes in their native conformation. As FDCs are thought to be long-lived cells, they are proposed to serve as a long-term repository of extracellular Ag important for induction and maintenance of memory responses (Mandel et al., 1980, 1981). The capacity of MRCs to generate columns of FDCs able to reach the center of GCs in reactive follicles raises two important issues. Are FDCs really long-lived cells, and if not, how can they behave as an antigenic repository? Our results indicate that in GCs, the great majority of FDCs derive from MRCs (Fig. 3 B), questioning the fate of the resident mature FDCs that were present at the initiation of the GC reaction. If the development of a humoral response implies that "experienced" FDCs loaded with previously encountered Ags are replaced by newly generated FDCs loaded with a different antigenic repertoire, one wonders how FDCs could retain Ag for long periods of time. FDCs have been reported to secrete and transfer immune complex coated bodies (iccosomes) to B cells (Szakal et al., 1988; Terashima et al., 1992). Iccosome-mediated exchange of Ag between experienced and newly generated FDCs would provide an efficient way to maintain a history of the antigenic repertoire on the FDC network without a need for long-lived FDCs. In addition, the maintenance of the antigenic repertoire may rely on the survival of few memory FDCs in charge of maintaining discrete reservoirs of antigen.

Our results identify MRCs as progenitor of LN FDCs, both during development and inflammation-induced remodeling. MRCs constitute a population of poorly characterized lymphoid stromal cells that reside in the outer edge of follicles and express RANK-L, CXCL13, gp38, and MAdCam-1 (Katakai, 2008, 2012). Based on phenotypical similarities, several groups raised the possibility that MRCs could descend from LTo (lymphoid tissue organizer) cells (Cupedo et al., 2004; Katakai et al., 2008) but formal proof is still lacking. As of today, no biological function has been assigned to MRCs, explaining why these cells represent one of the least understood lymphoid stromal cell subsets. Several pieces of indirect evidence suggested that MRCs may be involved in the establishment and/or the regulation of B cell follicles. For example, injection of RANK-L neutralizing antibodies to mouse embryos leads to disruption of B cell follicles with reduced B cell numbers and misplaced FDCs (Sugiyama et al., 2012) while postnatal RANK-L overexpression results in an increase in LN B cell follicles (Hess et al., 2012). As RANK-L is expressed by many cell types, including LTi cells known to be critical for LN development (Cupedo and Mebius, 2005; Koning and Mebius, 2012; Sugiyama et al., 2012), these studies did not specifically address the role of MRCs during B cell follicle development. The phenotypical resemblance of FDCs and MRCs combined to the aforementioned experiments also led to the hypothesis that MRCs could be the precursors of FDCs (Brendolan and Caamaño, 2012; Katakai, 2012; Mueller and Hess, 2012) but supporting evidence was critically lacking. Altogether, our results provide the formal demonstration that MRCs can give rise to LN FDCs during follicle development and inflammation-induced remodeling. Importantly, this study does not only shed light on the origin of LN FDCs but also reports the first biological function of MRCs.

Altogether, our results are fully consistent with a model in which MRCs proliferate before differentiating into mature FDCs. Although B cells appear to be mandatory to the differentiation of MRCs into FDCs, the presence of proliferative clusters of MRCs in RAG-2$^{-/-}$ Wnt-1Cre Ubow mice demonstrates that B cells are dispensable for MRC proliferation. If MRCs proliferate before LN colonization by B cells, which cell types regulate MRC proliferation? Blocking LTβR signaling causes loss of MAdCam-1 and CXCL13 expression on MRCs, indicating that the LT pathway is important for the maintenance of MRCs (Zindl et al., 2009). Interestingly, LTi cells express high levels of many tumor necrosis superfamily members, including LTβR ligands and RANK-L and are

located in the LN SCS and interfollicular areas (Lane et al., 2012). LTi cells may thus be fully equipped and ideally located to control LN MRC behavior but further experiments will be required to test this hypothesis.

Considering the unique localization of MRCs in LNs, it remains possible that MRC homeostasis could also be regulated by remotely secreted factors. MRCs are located immediately below the LN SCS and wrap around a conduit system able to convey lymphatic content within follicles (Bajénoff and Germain, 2009; Roozendaal et al., 2009). The lymphatic content is a potent modulator of stromal cell responses. For instance, when peripheral LNs are deprived of afferent lymph, high endothelial venules (HEVs), the entry gate of blood-derived lymphocytes in LNs, rapidly lose their ability to support lymphocyte trafficking (Hendriks and Eestermans, 1983; Drayson and Ford, 1984). Therefore, the establishment of the FDC network and its subsequent remodeling may rely on the capacity of MRCs to respond to unknown soluble or cellular material conveyed by afferent lymphatics.

Altogether, our study provides new insight into the cellular mechanisms driving the development and remodeling of LN FDCs while describing the first and pivotal biological function of MRCs as progenitors of LN FDCs. This study also demonstrates the ability of multicolor lineage tracing systems to unravel key features of stromal cell biology.

MATERIALS AND METHODS

Ethics statement. All procedures performed on animals in this study have been approved by the 14th national ethical committee of Marseille (France) under the reference 5–01022012.

Mice. C57BL/6J, Ubiquitin-CreERT2 (B6.Cg-Tg(UBC-cre/ERT2)1Ejb/J, strain 8085), CD21Cre (B6.Cg-Tg(Cr2-cre)3Cgn/J, strain 6368), μMt (B6.129S2-*Ighm*^{tm1Cgn}/J, strain 2288), and RAG-2$^{o/o}$ mice were purchased from The Jackson Laboratory. Wnt-1Cre mice were provided by M.C. Coles. Ubow mice were generated in the Service des Animaux Transgéniques (SEAT; Ghigo et al., 2013). For the generation of chimeras, mice were γ-irradiated (twice with 500 rad) from a cesium source and were reconstituted with BM cells as indicated in the main text (minimum of 2×10^6 BM cells per mouse). Chimeras were used at 8 wk after reconstitution. All mice were maintained in the CIML animal facilities and used between 6 and 12 wk unless indicated in the text.

Parabiosis. 10-wk-old WT and CD21Cre Ubow$^{+/-}$ μMT mice were surgically attached as described in Waskow (2010). Parabionts were analyzed 3 mo later.

Tamoxifen treatment. Tamoxifen and corn oil were purchased from Sigma-Aldrich. 3 mg tamoxifen was dissolved in corn oil and administered for 3 consecutive days i.p. At the end of the treatment, mice were maintained under tamoxifen-free regimen for 1 wk to eliminate tamoxifen residual activity (Fig. S3).

Immunostaining. LNs were harvested and fixed in AntigenFix (MMFrance) for 5 h, and then washed in phosphate buffer and dehydrated in 30% sucrose in phosphate buffer. 25- or 50-μm frozen sections were stained with the indicated antibodies as previously described (Bajénoff et al., 2003). EdU staining was performed using Click-it EdU Alexa Fluor 647 imaging kit (Life Technologies). Immunofluorescence confocal microscopy was performed with a confocal microscope (LSM 780; Carl Zeiss). Separate images were collected for each fluorochrome and overlaid to obtain a multicolor image. Final image processing was performed with Imaris software (Bitplane) and Photoshop (Adobe).

B cell adoptive transfer. Spleens harvested from C57BL/6 mice were digested with Collagenase I (Life Technologies) for 30 min at 37°C. Subsequent to red blood cell lysis, B cells were negatively isolated using a B cell isolation kit (purity >95%; Miltenyi Biotec). 6×10^7 B cells were injected intravenously via the orbital vein. When indicated, B cells were labeled with 0.5 μM CMFDA for 10 min at 37°C before transfer.

BrdU pulse-chase experiment. WT mice were injected three times with 1 mg BrdU i.p. with a 3-h interval. Mice were then maintained under a BrdU-free regimen for 1 or 3 additional days before analysis. BrdU was revealed using APC BrdU Flow kit (BD).

LN stromal cell dissociation and purification. All LNs (except mesenteric LNs) were digested as described in Fletcher et al. (2011). Stromal cell purification was performed using CD45 and CD31 microbeads (Miltenyi Biotec). Negatively selected LN cellular suspension was further blocked with anti CD16/32 Ab for 15 min at 4°C and stained with the indicated antibodies in PBS 1% FCS 2 mM EDTA for 45 min at 4°C. Data were acquired on FACSCanto II UV (BD) and were analyzed on DIVA software (BD).

Antibodies. 11-26c2a (anti-IgD), RA3-6B2 (anti-B220), 17A2 (anti-CD3), IK22.5 (anti–RANK-L), and 1D3 (anti-CD19) were purchased from BD. 8D9 (anti-CD21/35) and 8.1.1 (GP38) were purchased from eBioscience. 30F11 (CD45), 390 (CD31), and Meca-367 (MAdCam-1) were purchased from BioLegend. AF470 (anti-CXCL13) was purchased from R&D Systems. 18A2-G10 (anti-Mfge8) was purchased from MBL International. Anti-NG2 was purchased from Millipore. These antibodies were visualized by direct coupling to Pacific blue, allophycocyanin, and Alexa Fluor 488, 568, or 647; through the use of Alexa Fluor TSA kits; or through the use of Alexa Fluor 488, 568, 647, or biotin-coupled secondary antibodies (Life Technologies).

Quantification of FDC clustering. The quantification and statistical analysis of the spatial distribution of FDCs consists of three modules, which were all implemented with the CognitionMaster image analysis using C#/.NET. Computations were performed on standard hardware running Windows 7, 64 bit (Microsoft). In the first module, the different FDC classes are defined using the region-of-interest plugin (ROImanager) of the CognitionMaster, and the respective cells are labeled manually to obtain the cell center coordinate information for the subsequent processing step; the second module computes the 2D Voronoi mesh based on the manually labeled cell centers. The resulting tessellation establishes the neighborhood relationships between the cells, which is used to evaluate the number of cells (of the same type) assembled in clusters and the respective cluster sizes. Although this step provides a robust and objective means of cell cluster quantification, it does not yet allow for an assessment of the randomness or nonrandomness of the spatial cell distribution/cluster formation. To achieve this, in the final step, we use Monte Carlo simulations based on the cell numbers present in the corresponding experimental image data. In the 10,000 simulation runs we perform for each experimental dataset, the same numbers of cells as in the real images are randomly distributed over the same image areas, and for each simulation run, the spatial statistics (Voronoi mesh, neighborhood, and cell cluster features) are computed in the same way as for the experimentally obtained images. After all simulation runs are completed, we compare the results of the spatial statistics of the real and simulated data. The ratio between the number of simulations in which the mean cluster size is larger than in the real data and the total number of Monte Carlo simulations (here: 10,000) yields the p-values indicating the probability that an experimentally observed cluster formation may as well have been achieved by random cell distribution (for details see Fig. S1).

FDC-MRC-cluster analysis. To provide a quantitative analysis of the question of whether FDCs associate with MRCs of the same color in the inflamed follicles of Ubow$^{+/+}$ CreERT2 chimeric mice treated with tamoxifen (Fig. 3), we used 23 samples, which showed MRC-FDC-cluster formation. We defined a cluster as being a group of at least five contiguous MRCs and

FDCs of the same color. Unrecombined Tomato/Tomato cells were excluded from the cluster analysis because of their high frequency and high capacity to associate in cluster randomly. We manually labeled all the colored FDCs and MRCs present in the follicles using the above described software tool. FDC and MRC areas were then delineated manually based on CD21/35 and RANK-L stainings and served as the regions of interest for the subsequent computational analysis. To measure the association of MRCs and FDCs sharing a similar color in columnar structures, we computed a cell clustering measure slightly different from the one used above. For each cell present in a monocolored MRC/FDC cluster, we determined the proportion of its neighbors that had a similar color (e.g., in a YFP/YFP cluster, a cell that has two YFP-YFP, two Tomato-CFP, and two CFP-CFP neighbors has a ratio of 1/3). We then averaged the ratio of all cells present in a given cluster to obtain the "clustering index" of this cluster. This index is larger than 0 and smaller than 1 because cells at a cluster border always have neighboring cells of a different color. The clustering index was first computed for the original data and provided a measure of the compactness of MRC/FDC clusters ($\sim$1 = extremely compact, $\sim$0 = not compact). Second, we performed Monte Carlo simulations (see above) in which the same number of FDCs as in the original data is distributed randomly in the FDC region (MRCs were not redistributed in Monte-Carlo simulations). The clustering index was computed for each simulation run and the final clustering index of the simulated data was the mean over 10,000 simulations. The number of simulations *np* in which the clustering index is the same or higher than in the corresponding original dataset is used to determine the error probability and thus the significance of the results: p-value = (*np*/10,000). (For details, see Fig. S2.)

Quantification of MRC expansion upon B cell transfer in RAG-2–deficient mice. Immunofluorescence images were used to delineate RANK-L$^+$ MRC regions and calculate their surface and mean width with ImageJ software (National Institutes of Health). The number of RANK-L$^+$ dTomato$^+$ cellular bodies was then manually counted for each MRC area and used to calculate the density of MRCs per mm^2 of MRC area.

Estimation of residual tamoxifen activity in vivo. WT mice were treated with tamoxifen (3 mg administered for 3 consecutive days i.p). Mice were maintained in a tamoxifen-free regimen for an additional period of 1, 3, or 7 d and then received 10^7 total LN cells (i.v.) isolated from a Ubow^{++} CreRT2 mouse. 1 wk later, the colors of the adoptively transferred T and B cells were analyzed by flow cytometry (Fig. S3).

Online supplemental material. Figs. S1 and S2 explain the quantification of FDC and FDC/MRC clustering. Fig. S3 shows residual tamoxifen activity in vivo. Video 1 displays several examples of MRC/FDC columns in the inflamed LNs of Ubow Cre ERT2 chimeras treated with tamoxifen. Online supplemental material is available at http://www.jem.org/cgi/content/full/jem.20132409/DC1.

We thank Jean Livet for providing the brainbow 1.0L construct, Clément Ghigo and Jonathan Nowak for technical help, Emilie Narni-Mancinelli and Toby Lawrence for scientific comments and discussions, and the ImagImm photonic microscopy facility of the CIML.

This work was supported by grants from the Agence Nationale de la Recherche (ANR; ANR-RCS, ANR-STROMA, and ANR-10-INBS-04-01 France Bio Imaging), the Medical Research Council (MRC G0601156), and the Human Frontier Science Program (Young Investigator Grants RGY0077/2011 and RGP006/2009).

The authors have no conflicting financial interests.

Author contributions: M. Jarjour, I. Mondor, A. Jorquera, S. Wienert, and P. Narang performed the experiments. F. Klauschen, M. Jarjour, M.C. Coles, and M. Bajénoff designed the experiments and wrote the manuscript.

Submitted: 20 November 2013
Accepted: 14 April 2014

REFERENCES

Allen, C.D., and J.G. Cyster. 2008. Follicular dendritic cell networks of primary follicles and germinal centers: phenotype and function. *Semin. Immunol.* 20:14–25. http://dx.doi.org/10.1016/j.smim.2007.12.001

Allen, C.D., K.M. Ansel, C. Low, R. Lesley, H. Tamamura, N. Fujii, and J.G. Cyster. 2004. Germinal center dark and light zone organization is mediated by CXCR4 and CXCR5. *Nat. Immunol.* 5:943–952. http://dx.doi.org/10.1038/ni1100

Allen, C.D., T. Okada, and J.G. Cyster. 2007. Germinal-center organization and cellular dynamics. *Immunity*. 27:190–202. http://dx.doi.org/10.1016/j.immuni.2007.07.009

Ansel, K.M., V.N. Ngo, P.L. Hyman, S.A. Luther, R. Förster, J.D. Sedgwick, J.L. Browning, M. Lipp, and J.G. Cyster. 2000. A chemokine-driven positive feedback loop organizes lymphoid follicles. *Nature*. 406:309–314. http://dx.doi.org/10.1038/35018581

Bajénoff, M., and R.N. Germain. 2009. B-cell follicle development remodels the conduit system and allows soluble antigen delivery to follicular dendritic cells. *Blood*. 114:4989–4997. http://dx.doi.org/10.1182/blood-2009-06-229567

Bajénoff, M., S. Granjeaud, and S. Guerder. 2003. The strategy of T cell antigen–presenting cell encounter in antigen-draining lymph nodes revealed by imaging of initial T cell activation. *J. Exp. Med.* 198:715–724. http://dx.doi.org/10.1084/jem.20030167

Bajénoff, M., J.G. Egen, L.Y. Koo, J.P. Laugier, F. Brau, N. Glaichenhaus, and R.N. Germain. 2006. Stromal cell networks regulate lymphocyte entry, migration, and territoriality in lymph nodes. *Immunity*. 25:989–1001. http://dx.doi.org/10.1016/j.immuni.2006.10.011

Brendolan, A., and J.H. Caamaño. 2012. Mesenchymal cell differentiation during lymph node organogenesis. *Front Immunol.* 3:381. http://dx.doi.org/10.3389/fimmu.2012.00381

Castagnaro, L., E. Lenti, S. Maruzzelli, L. Spinardi, E. Migliori, D. Farinello, G. Sitia, Z. Harrelson, S.M. Evans, L.G. Guidotti, et al. 2013. Nkx2-5$^+$islet1$^+$ mesenchymal precursors generate distinct spleen stromal cell subsets and participate in restoring stromal network integrity. *Immunity*. 38:782–791. http://dx.doi.org/10.1016/j.immuni.2012.12.005

Chen, L.L., A.M. Frank, J.C. Adams, and R.M. Steinman. 1978. Distribution of horseradish peroxidase (HRP)-anti-HRP immune complexes in mouse spleen with special reference to follicular dendritic cells. *J. Cell Biol.* 79:184–199. http://dx.doi.org/10.1083/jcb.79.1.184

Cupedo, T., and R.E. Mebius. 2005. Cellular interactions in lymph node development. *J. Immunol.* 174:21–25. http://dx.doi.org/10.4049/jimmunol.174.1.21

Cupedo, T., M.F. Vondenhoff, E.J. Heeregrave, A.E. De Weerd, W. Jansen, D.G. Jackson, G. Kraal, and R.E. Mebius. 2004. Presumptive lymph node organizers are differentially represented in developing mesenteric and peripheral nodes. *J. Immunol.* 173:2968–2975. http://dx.doi.org/10.4049/jimmunol.173.5.2968

Cyster, J.G., K.M. Ansel, K. Reif, E.H. Ekland, P.L. Hyman, H.L. Tang, S.A. Luther, and V.N. Ngo. 2000. Follicular stromal cells and lymphocyte homing to follicles. *Immunol. Rev.* 176:181–193. http://dx.doi.org/10.1034/j.1600-065X.2000.00618.x

Drayson, M.T., and W.L. Ford. 1984. Afferent lymph and lymph borne cells: their influence on lymph node function. *Immunobiology*. 168:362–379. http://dx.doi.org/10.1016/S0171-2985(84)80123-0

Endres, R., M.B. Alimzhanov, T. Plitz, A. Fütterer, M.H. Kosco-Vilbois, S.A. Nedospasov, K. Rajewsky, and K. Pfeffer. 1999. Mature follicular dendritic cell networks depend on expression of lymphotoxin β receptor by radioresistant stromal cells and of lymphotoxin β and tumor necrosis factor by B cells. *J. Exp. Med.* 189:159–168. http://dx.doi.org/10.1084/jem.189.1.159

Fletcher, A.L., D. Malhotra, S.E. Acton, V. Lukacs-Kornek, A. Bellemare-Pelletier, M. Curry, M. Armant, and S.J. Turley. 2011. Reproducible isolation of lymph node stromal cells reveals site-dependent differences in fibroblastic reticular cells. *Front Immunol.* 2:35. http://dx.doi.org/10.3389/fimmu.2011.00035

Fu, Y.X., G. Huang, Y. Wang, and D.D. Chaplin. 1998. B lymphocytes induce the formation of follicular dendritic cell clusters in a lymphotoxin α-dependent fashion. *J. Exp. Med.* 187:1009–1018. http://dx.doi.org/10.1084/jem.187.7.1009

Garin, A., M. Meyer-Hermann, M. Contie, M.T. Figge, V. Buatois, M. Gunzer, K.M. Toellner, G. Elson, and M.H. Kosco-Vilbois. 2010. Toll-like receptor 4 signaling by follicular dendritic cells is pivotal for germinal center onset and affinity maturation. *Immunity*. 33:84–95. http://dx.doi.org/10.1016/j.immuni.2010.07.005

Ghigo, C., I. Mondor, A. Jorquera, J. Nowak, S. Wienert, S.P. Zahner, B.E. Clausen, H. Luche, B. Malissen, F. Klauschen, and M. Bajénoff. 2013. Multicolor fate mapping of Langerhans cell homeostasis. *J. Exp. Med.* 210:1657–1664. http://dx.doi.org/10.1084/jem.20130403

Hayashi, S., and A.P. McMahon. 2002. Efficient recombination in diverse tissues by a tamoxifen-inducible form of Cre: a tool for temporally regulated gene activation/inactivation in the mouse. *Dev. Biol.* 244:305–318. http://dx.doi.org/10.1006/dbio.2002.0597

Hendriks, H.R., and I.L. Eestermans. 1983. Disappearance and reappearance of high endothelial venules and immigrating lymphocytes in lymph nodes deprived of afferent lymphatic vessels: a possible regulatory role of macrophages in lymphocyte migration. *Eur. J. Immunol.* 13:663–669. http://dx.doi.org/10.1002/eji.1830130811

Hess, E., V. Duheron, M. Decossas, F. Lézot, A. Berdal, S. Chea, R. Golub, M.R. Bosisio, S.L. Bridal, Y. Choi, et al. 2012. RANKL induces organized lymph node growth by stromal cell proliferation. *J. Immunol.* 188:1245–1254. http://dx.doi.org/10.4049/jimmunol.1101513

Jiang, X., D.H. Rowitch, P. Soriano, A.P. McMahon, and H.M. Sucov. 2000. Fate of the mammalian cardiac neural crest. *Development*. 127:1607–1616.

Katakai, T. 2012. Marginal reticular cells: a stromal subset directly descended from the lymphoid tissue organizer. *Front Immunol.* 3:200. http://dx.doi.org/10.3389/fimmu.2012.00200

Katakai, T., H. Suto, M. Sugai, H. Gonda, A. Togawa, S. Suematsu, Y. Ebisuno, K. Katagiri, T. Kinashi, and A. Shimizu. 2008. Organizer-like reticular stromal cell layer common to adult secondary lymphoid organs. *J. Immunol.* 181:6189–6200. http://dx.doi.org/10.4049/jimmunol.181.9.6189

Kitamura, D., J. Roes, R. Kühn, and K. Rajewsky. 1991. A B cell-deficient mouse by targeted disruption of the membrane exon of the immunoglobulin μ chain gene. *Nature*. 350:423–426. http://dx.doi.org/10.1038/350423a0

Klaus, G.G., J.H. Humphrey, A. Kunkl, and D.W. Dongworth. 1980. The follicular dendritic cell: its role in antigen presentation in the generation of immunological memory. *Immunol. Rev.* 53:3–28. http://dx.doi.org/10.1111/j.1600-065X.1980.tb01038.x

Koning, J.J., and R.E. Mebius. 2012. Interdependence of stromal and immune cells for lymph node function. *Trends Immunol.* 33:264–270. http://dx.doi.org/10.1016/j.it.2011.10.006

Krautler, N.J., V. Kana, J. Kranich, Y. Tian, D. Perera, D. Lemm, P. Schwarz, A. Armulik, J.L. Browning, M. Tallquist, et al. 2012. Follicular dendritic cells emerge from ubiquitous perivascular precursors. *Cell*. 150:194–206. http://dx.doi.org/10.1016/j.cell.2012.05.032

Lane, P.J., F.M. Gaspal, F.M. McConnell, D.R. Withers, and G. Anderson. 2012. Lymphoid tissue inducer cells: pivotal cells in the evolution of CD4 immunity and tolerance? *Front Immunol.* 3:24. http://dx.doi.org/10.3389/fimmu.2012.00024

Livet, J., T.A. Weissman, H. Kang, R.W. Draft, J. Lu, R.A. Bennis, J.R. Sanes, and J.W. Lichtman. 2007. Transgenic strategies for combinatorial expression of fluorescent proteins in the nervous system. *Nature*. 450:56–62. http://dx.doi.org/10.1038/nature06293

MacLennan, I.C. 1994. Germinal centers. *Annu. Rev. Immunol.* 12:117–139. http://dx.doi.org/10.1146/annurev.iy.12.040194.001001

Mandel, T.E., R.P. Phipps, A. Abbot, and J.G. Tew. 1980. The follicular dendritic cell: long term antigen retention during immunity. *Immunol. Rev.* 53:29–59. http://dx.doi.org/10.1111/j.1600-065X.1980.tb01039.x

Mandel, T.E., R.P. Phipps, A.P. Abbot, and J.G. Tew. 1981. Long-term antigen retention by dendritic cells in the popliteal lymph node of immunized mice. *Immunology*. 43:353–362.

Mionnet, C., I. Mondor, A. Jorquera, M. Loosveld, J. Maurizio, M.L. Arcangeli, N.H. Ruddle, J. Nowak, M. Aurrand-Lions, H. Luche, and M. Bajénoff. 2013. Identification of a new stromal cell type involved in the regulation of inflamed B cell follicles. *PLoS Biol.* 11:e1001672. http://dx.doi.org/10.1371/journal.pbio.1001672

Mueller, C.G., and E. Hess. 2012. Emerging functions of RANKL in lymphoid tissues. *Front Immunol.* 3:261. http://dx.doi.org/10.3389/fimmu.2012.00261

Muñoz-Fernández, R., F.J. Blanco, C. Frecha, F. Martín, M. Kimatrai, A.C. Abadía-Molina, J.M. García-Pacheco, and E.G. Olivares. 2006. Follicular dendritic cells are related to bone marrow stromal cell progenitors and to myofibroblasts. *J. Immunol.* 177:280–289. http://dx.doi.org/10.4049/jimmunol.177.1.280

Quante, M., S.P. Tu, H. Tomita, T. Gonda, S.S. Wang, S. Takashi, G.H. Baik, W. Shibata, B. Diprete, K.S. Betz, et al. 2011. Bone marrow-derived myofibroblasts contribute to the mesenchymal stem cell niche and promote tumor growth. *Cancer Cell*. 19:257–272. http://dx.doi.org/10.1016/j.ccr.2011.01.020

Roozendaal, R., T.R. Mempel, L.A. Pitcher, S.F. Gonzalez, A. Verschoor, R.E. Mebius, U.H. von Andrian, and M.C. Carroll. 2009. Conduits mediate transport of low-molecular-weight antigen to lymph node follicles. *Immunity*. 30:264–276. http://dx.doi.org/10.1016/j.immuni.2008.12.014

Snippert, H.J., L.G. van der Flier, T. Sato, J.H. van Es, M. van den Born, C. Kroon-Veenboer, N. Barker, A.M. Klein, J. van Rheenen, B.D. Simons, and H. Clevers. 2010. Intestinal crypt homeostasis results from neutral competition between symmetrically dividing Lgr5 stem cells. *Cell*. 143:134–144. http://dx.doi.org/10.1016/j.cell.2010.09.016

Sugiyama, M., G. Nakato, T. Jinnohara, H. Akiba, K. Okumura, H. Ohno, and H. Yoshida. 2012. Expression pattern changes and function of RANKL during mouse lymph node microarchitecture development. *Int. Immunol.* 24:369–378. http://dx.doi.org/10.1093/intimm/dxs002

Szakal, A.K., and M.G. Hanna Jr. 1968. The ultrastructure of antigen localization and viruslike particles in mouse spleen germinal centers. *Exp. Mol. Pathol.* 8:75–89. http://dx.doi.org/10.1016/0014-4800(68)90007-5

Szakal, A.K., M.H. Kosco, and J.G. Tew. 1988. A novel in vivo follicular dendritic cell-dependent iccosome-mediated mechanism for delivery of antigen to antigen-processing cells. *J. Immunol.* 140:341–353.

Tabansky, I., A. Lenarcic, R.W. Draft, K. Loulier, D.B. Keskin, J. Rosains, J. Rivera-Feliciano, J.W. Lichtman, J. Livet, J.N. Stern, et al. 2013. Developmental bias in cleavage-stage mouse blastomeres. *Curr. Biol.* 23:21–31. http://dx.doi.org/10.1016/j.cub.2012.10.054

Takahashi, K., Y. Kozono, T.J. Waldschmidt, D. Berthiaume, R.J. Quigg, A. Baron, and V.M. Holers. 1997. Mouse complement receptors type 1 (CR1;CD35) and type 2 (CR2;CD21): expression on normal B cell subpopulations and decreased levels during the development of autoimmunity in MRL/lpr mice. *J. Immunol.* 159:1557–1569.

Terashima, K., M. Dobashi, K. Maeda, and Y. Imai. 1992. Follicular dendritic cell and ICCOSOMES in germinal center reactions. *Semin. Immunol.* 4:267–274.

Usui, K., S. Honda, Y. Yoshizawa, C. Nakahashi-Oda, S. Tahara-Hanaoka, K. Shibuya, and A. Shibuya. 2012. Isolation and characterization of naïve follicular dendritic cells. *Mol. Immunol.* 50:172–176. http://dx.doi.org/10.1016/j.molimm.2011.11.010

van Rees, E.P., E.A. Döpp, C.D. Dijkstra, and T. Sminia. 1985. The postnatal development of cell populations in the rat popliteal lymph node. An immunohistochemical study. *Cell Tissue Res.* 242:391–398.

Victora, G.D., and M.C. Nussenzweig. 2012. Germinal centers. *Annu. Rev. Immunol.* 30:429–457. http://dx.doi.org/10.1146/annurev-immunol-020711-075032

Wang, X., B. Cho, K. Suzuki, Y. Xu, J.A. Green, J. An, and J.G. Cyster. 2011. Follicular dendritic cells help establish follicle identity and promote B cell retention in germinal centers. *J. Exp. Med.* 208:2497–2510. http://dx.doi.org/10.1084/jem.20111449

Waskow, C. 2010. Generation of parabiotic mice for the study of DC and DC precursor circulation. *Methods Mol. Biol.* 595:413–428. http://dx.doi.org/10.1007/978-1-60761-421-0_27

Wilke, G., G. Steinhauser, J. Grün, and C. Berek. 2010. In silico subtraction approach reveals a close lineage relationship between follicular dendritic cells and BP3(hi) stromal cells isolated from SCID mice. *Eur. J. Immunol.* 40:2165–2173. http://dx.doi.org/10.1002/eji.200940202

Zindl, C.L., T.H. Kim, M. Zeng, A.S. Archambault, M.H. Grayson, K. Choi, R.D. Schreiber, and D.D. Chaplin. 2009. The lymphotoxin $LT\alpha_1\beta_2$ controls postnatal and adult spleen marginal sinus vascular structure and function. *Immunity*. 30:408–420. http://dx.doi.org/10.1016/j.immuni.2009.01.010